Title

Thickness-dependent magnetic and electrical transport properties of epitaxial La0.7Sr0.3CoO3 films

Journal

AIP Advances, 7(4)

ISSN

2158-3226

Authors

Li, Binzhi

Chopdekar, Rajesh V

Kane, Alexander M

et al.

Publication Date

2017-04-01

DOI

10.1063/1.4979921

Peer reviewed

Thickness-dependent magnetic and electrical transport properties of epitaxial $La_{0.7}Sr_{0.3}CoO_3$ films

Binzhi Li, Rajesh V. Chopdekar, Alexander M. Kane, Kyle Hoke, Alpha T. N'Diaye, Elke Arenholz, and Yayoi Takamura

Citation: AIP Advances **7**, 045003 (2017); doi: 10.1063/1.4979921
View online: http://dx.doi.org/10.1063/1.4979921
View Table of Contents: http://aip.scitation.org/toc/adv/7/4
Published by the American Institute of Physics

Thickness-dependent magnetic and electrical transport properties of epitaxial $La_{0.7}Sr_{0.3}CoO_3$ films

Binzhi Li,[1] Rajesh V. Chopdekar,[1] Alexander M. Kane,[1] Kyle Hoke,[1] Alpha T. N'Diaye,[2] Elke Arenholz,[2] and Yayoi Takamura[1,a]
[1]*Department of Materials Science and Engineering, University of California, Davis, Davis, California 95616, USA*
[2]*Advanced Light Source, Lawrence Berkeley National Laboratory, Berkeley, California 94720, USA*

(Received 9 November 2016; accepted 27 March 2017; published online 4 April 2017)

The thickness-dependent magnetic and electrical transport properties of nearly strain-free $La_{0.7}Sr_{0.3}CoO_3$ (LSCO) films grown on (001)-oriented $(LaAlO_3)_{0.3}(Sr_2AlTaO_6)_{0.7}$ substrates were systematically studied. A crossover from ferromagnetic/metallic to non-magnetic/insulating behavior occurs at a critical thickness (~8 nm) that is significantly smaller than LSCO films under larger strains in reported literature. X-ray absorption measurements revealed that the difference of functional properties at reduced film thicknesses was accompanied by changes in the valence state of Co ions at the film/substrate interface. [http://dx.doi.org/10.1063/1.4979921]

Sr-doped lanthanum cobaltites ($La_{1-x}Sr_xCoO_3$) are the topic of extensive research due to their rich phase diagram of electronic and magnetic properties depending on the Sr doping level, x, as well as their potential application in spintronic devices.[1–3] At low doping levels ($0 < x < 0.18$), bulk $La_{1-x}Sr_xCoO_3$ displays magneto-electronic phase separation (MEPS) that evolves from a spin-glass state to a percolated ferromagnetic (FM) state with increasing Sr concentration.[4–8] In this regime, $La_{1-x}Sr_xCoO_3$ consists of small clusters of an FM/metallic phase, which originates from the Co^{3+}-O-Co^{4+} double-exchange mechanism, embedded in an antiferromagnetic/insulating matrix that results from a Co^{3+}-O-Co^{3+} and Co^{4+}-O-Co^{4+} superexchange interactions.[3] The FM clusters grow both in size and in concentration with increasing x and eventually percolate to form long-range FM ordering. Such phenomenon is usually discussed in terms of the small energy gap between the t_{2g} and e_g orbitals for the Co ions, which subsequently results in spin-state transitions (e.g. between low-spin, intermediate-spin and high-spin states) that can be tuned by Sr concentration or thermal energy.[9,10]

Factors such as growth conditions, epitaxial strain imposed by the underlying substrate, and film thickness have been shown to significantly alter the functional properties of $La_{1-x}Sr_xCoO_3$ films.[11–16] For example, Torija *et al.*[17] reported the altered magnetic and electrical transport properties of several $La_{1-x}Sr_xCoO_3$ compositions grown on (001)-oriented $SrTiO_3$ (STO) substrates when the thickness was reduced below a critical value. This critical thickness increased as the Sr concentration decreased, with a value of 15 nm for $La_{1-x}Sr_xCoO_3$ (x=0.28) thin films with 1.8% tensile strain. Similar results were found on other cobaltites such as (001)-oriented $Nd_{0.5}Sr_{0.5}CoO_3$ (NSCO)/STO thin films with 2.43% tensile strain, where the change of magnetic properties was accompanied with a large enhancement of coercivity for thicknesses below 7 nm.[18] These thickness-dependent properties of cobaltite thin films have been discussed in the context of the formation of oxygen vacancies at the film/substrate interface. Long-range ordering of oxygen vacancies in $La_{1-x}Sr_xCoO_3$ films[14,18,19] was found to depend on the sign and magnitude of the epitaxial strain as well as the substrate orientation. In the present study, epitaxial

[a]Corresponding author, email: ytakamura@ucdavis.edu

$La_{0.7}Sr_{0.3}CoO_3$ (LSCO) thin films were grown on (001)-oriented $(LaAlO_3)_{0.3}$ $(Sr_2AlTaO_6)_{0.7}$ (LSAT) substrates in an effort to explore the thickness dependence of their functional properties with a minimal tensile lattice strain of 0.6%. These results will enable the development of comprehensive models to predict the magnetic and electrical properties of $La_{1-x}Sr_xCoO_3$ films under arbitrary sample geometries, including the effect of factors such as epitaxial strain, composition, and film thickness.

LSCO thin films were grown epitaxially on (001)-oriented LSAT substrates by pulsed laser deposition. The film thicknesses were designed to be 2 nm, 4 nm, 8 nm, and 12 nm, which are denoted as samples C2, C4, C8, and C12, respectively. During growth, the substrate temperature was held at 700 °C, the oxygen pressure was 0.3 Torr, and a 248 nm wavelength laser energy of 1.2 J/cm^2 and repetition rate of 5 Hz were used. To assure proper oxygen stoichiometry, the samples were cooled slowly to room temperature in a 300 Torr oxygen atmosphere after the growth. For comparison, LSCO films were also grown using the same grown conditions on (001)-oriented STO substrates.

The structural properties of the thin films were characterized using x-ray reflectivity (XRR) and high-resolution x-ray diffraction (XRD) using a Bruker D8 Discover 4-circle diffractometer. The strain states of all samples were investigated using reciprocal space maps (RSMs) around the (103) reflections. Macroscopic magnetization was studied using a Quantum Design superconducting quantum interference device (SQUID) magnetometer with the magnetic field applied along the in-plane [100] substrate direction. Element specific electronic structure and magnetic characterization was obtained using x-ray absorption (XA) and x-ray magnetic circular dichroism (XMCD), respectively. The XA/XMCD spectra were acquired at beamline 6.3.1 of the Advanced Light Source (ALS) in total-electron-yield (TEY) mode at 80 K. Due to the finite escape depth of the secondary electrons detected in TEY mode (4-10 nm),[20] these spectra provide greater chemical and magnetic sensitivity to the portion of the film at the air-film interface as compared to the portion of the film near the film-substrate interface. The applied magnetic field direction was collinear with the x-ray beam that impinged on the sample surface at 60 degrees to the surface normal with the in-plane component along the in-plane [100] substrate direction. Electrical transport properties were measured using a Quantum Design Physical Property Measurement System. The electrical resistance of the LSCO films was measured using a four-terminal sensing geometry. All measurements were performed during the warming cycle between 10 - 350 K.

Figure 1(a) shows XRD ω-2θ scans around the substrate and film (002) reflections for samples C4, C8, and C12. The film peak intensity from sample C2 was too weak to be measured. A clear film peak and the presence of Kiessig fringes in all curves reveal that the LSCO layers are highly crystalline and single-phase. The layer thickness, density, and roughness were determined by fitting the ω-2θ scans and XRR spectra (not shown) using the Bruker Leptos software.[21] The fits demonstrate that the changes in the film peak width and periodicity of the Kiessig fringes correspond to the individual thicknesses of each sample, and that the layer thicknesses were within 10% deviation of

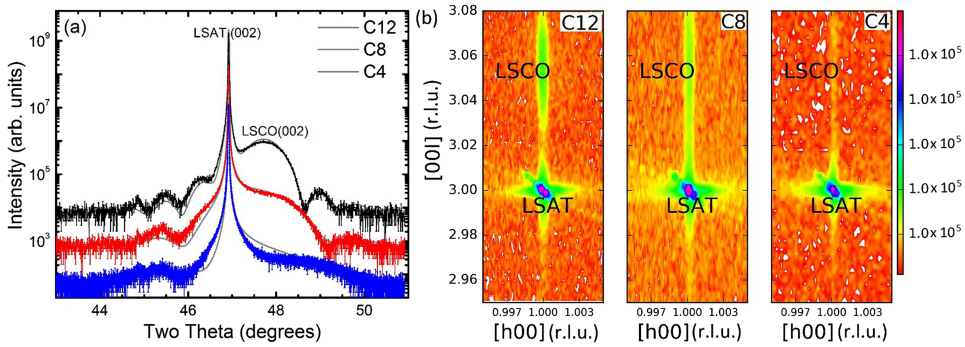

FIG. 1. (a) ω-2θ XRD scans around the (002) peaks and (b) RSMs around the (103) peaks for samples C4, C8, and C12. The grey lines in (a) represent fits showing that the peak width and periodicity of the Kiessig fringes correspond to the individual layer thicknesses of the samples.

their respective nominal thickness while the interface roughness was below 0.5 nm. RSMs around the (103) peaks for samples C4, C8, and C12 (Figure 1(b)) show fully epitaxial growth of the LSCO layers on the (001)-oriented LSAT substrates, as the full width at half maximum of the film peak was within a factor 2.5 of that of the substrate peak.

Magnetization vs. temperature ($M(T)$) curves measured by SQUID magnetometry are shown in Figure 2(a–c). Both 0.2 T field-cooled (FC) and zero-field-cooled (ZFC) curves were taken upon warming in a measurement field of 0.2 T. A bifurcation between the ZFC and FC curves can be observed in samples C12 and C8 as typically found in spin-glassy materials such as LSCO. Previous studies on LSCO have correlated this bifurcation to the existence of FM clusters in a non-magnetic matrix.[22–24] The field cooling aligns all the FM clusters in the direction of the applied field, while they are randomly aligned in the ZFC case in a manner that is dictated by the local anisotropy field with no long-range magnetic order. The FC curves for samples C12 and C8 show typical Brillouin-like FM temperature dependence. The Curie temperature (T_c) was determined to be ~175 K for samples C8 and C12 from the FC curves at the peak in dM/dT (indicated by the dotted lines in Figure 2(a) and (b)). The peak in the ZFC curves (freezing temperature, T_f, denoted with the downward arrow in Fig. 2(a) and (b)) can be interpreted as the point where the competition between the local anisotropy field and the applied magnetic field was balanced. T_f decreased from 168 K to 138 K for samples C12 to C8. For samples C2 and C4, minimum magnetization values were obtained indicating weak FM ordering throughout the temperature range studied.

Figure 2 (d–f) plots the temperature-dependent resistivity ($\rho(T)$) of the LSCO thin films. The sheet resistance of sample C2 exceeded the maximum value of the experimental setup (5 GOhm) at room temperature. The resistivity values follow a trend of increasing resistivity with decreasing film thickness over the temperature range investigated. For sample C12, $\rho(T)$ displayed a crossover from insulating ($d\rho/dT < 0$) to metallic ($d\rho/dT > 0$) behavior followed by an upturn of resistivity upon further cooling to 10 K. The metal-to-insulator transition temperature can be extracted from the peak in $d\rho/dT$ (126 K for sample C12), slightly below the $T_C = 175$ K derived from the $M(T)$ curve as has been previously observed for $La_{1-x}Sr_xCoO_3$.[24] For sample C8, no clear metallic region can be observed, though a change in slope between 100 – 200 K with a rapid increase in resistivity below 100 K can be observed. Finally, for sample C4, the insulating behavior fully dominates in the entire measured temperature range. These results confirm the crossover from metallic to insulating electrical behavior with decreasing LSCO thickness as was previously reported for LSCO and NSCO films grown on STO substrates.[11,18]

The magnetic switching behavior of the LSCO films was investigated using SQUID magnetometry as shown in Figure 3. The diamagnetic background from the LSAT substrate was subtracted

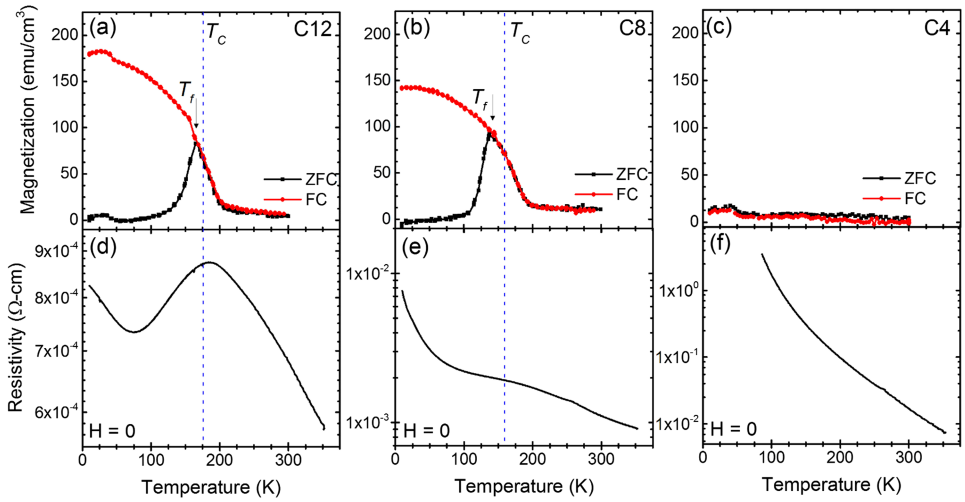

FIG. 2. (a-c) ZFC and FC $M(T)$ curves. The magnetic field applied during field cooling and measurements was 0.2 T. (d-f) $\rho(T)$ curves under zero magnetic field for samples C12, C8, and C4. Downward arrows denote T_f, while the vertical dashed lines refer to T_C extracted from maximum slope of $M(T)$ vs T curves.

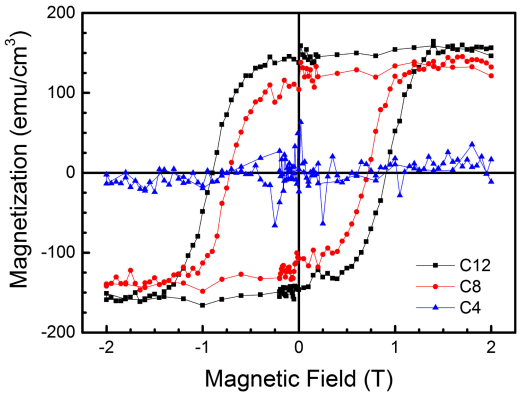

FIG. 3. Magnetic hysteresis loops at 80 K for samples C4, C8, and C12 measured by SQUID magnetometry.

from the total measured SQUID signal. A change in the magnetic properties with reduced film thickness can be clearly observed. The saturation magnetization (M_S) for sample C12 (~150 emu/cm^3) is close to that of the bulk LSCO,[3] while it decreases to 125 emu/cm^3 when the thickness is reduced to 8 nm. At the same time, the coercive field decreases from 0.90 T to 0.72 T, compared to reported values bulk LSCO ~0.003 T.[3] Similar large enhancements in coercivity in $La_{1-x}Sr_xCoO_3$/STO[17] and NSCO/STO[18] thin films were attributed to domain wall pinning in the MEPS layer. Samples C4 and C2 only show the diamagnetic signal from the substrate, as the magnetic moment from the samples is below the detection limit (10^{-6} emu) of the SQUID magnetometer.

The magnetic and electrical transport measurements both indicate a gradual change in ferromagnetic and metallic behavior in LSCO thin films as the film thickness decreases. These results provide evidence for a layer with non-magnetic and insulating behavior that lies at the LSCO/LSAT interface as was found previously in the $La_{1-x}Sr_xCoO_3$/STO[17] and NSCO/STO[18] systems. Specifically in the case of $La_{0.72}Sr_{0.28}CoO_3$ with a 1.8% tensile strain, Torija *et al.*[17] found that the crossover from the FM/metallic to non-magnetic/insulating state occurred at a critical thickness, $t^* = 15$ nm. In this case t^* was defined as the thickness where M_S was suppressed significantly, while T_C remained near bulk values. Figure 4 plots T_C and M_S for the LSCO films grown on LSAT and STO substrates from the

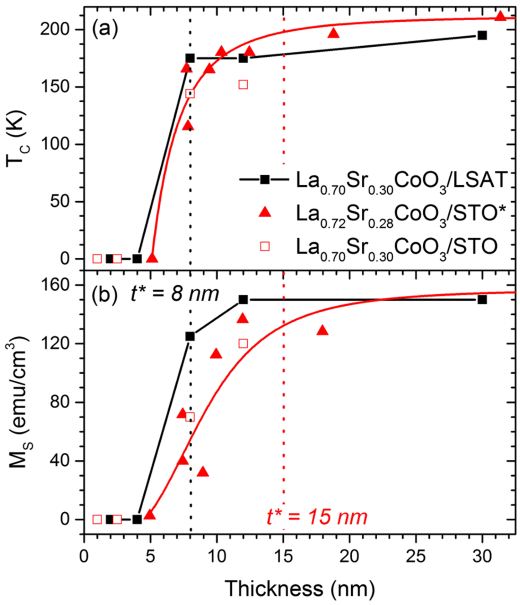

FIG. 4. (a) T_C and (b) M_S as a function of film thickness for the LSCO films grown on LSAT and STO substrates from this work and $La_{0.72}Sr_{0.28}CoO_3$ films grown on STO substrates from Torija *et al.*[17] M_S from the current work was measured at 80 K, and 10 K from Torija *et al.* The solid lines are guides to the eye and vertical lines are the t^* values.

current work. For comparison, the data for the $La_{0.72}Sr_{0.28}CoO_3$/STO system from Torija *et al.*[17] has also been plotted. From this analysis, we can define $t^* = 8$ nm for the nearly strain-free LSCO/LSAT system, indicating that epitaxial strain plays a strong role in the formation of the non-magnetic layer.

The origin of this non-magnetic layer in the (001)-oriented LSCO/LSAT films can be gleaned from careful analysis of the XA/XMCD spectra shown in Figure 5. XA spectra are sensitive to details of the electronic structure related to the Co valence states (Co^{2+}, Co^{3+}, and Co^{4+}) and the local bonding configuration (e.g. tetrahedral vs. octahedral site symmetry), while the XMCD spectra provide information on the valence states of the FM species. The evolution of the Co-XA and XMCD spectra with varying LSCO thickness follows the same trend as the macroscopically averaged magnetic and electrical transport properties as described above. The Co-XA and XMCD spectra for samples C12 and C8 show almost no variation and share all of the spectral features of thick LSCO films where the interface contributions are negligible. The magnitude of the XMCD displays a similar thickness dependence as that seen with SQUID magnetometry. Due to the highly resistive nature of sample C2, XMCD spectra could not be acquired at 80 K. The thinner films show changes in the electronic structure: the main feature (P_2) on the L_3 edge shifts to lower energy (by 0.2 eV for sample C4, and 0.4 eV sample C2), and the P_3/P_4 intensity ratio increases at the L_2 edge. Comparison of all four spectra indicate that the LSCO films have an increased concentration of Co^{3+} ions in the region close to the LSAT substrate.[25,26] The presence of the pre-edge feature (P_1) on the L_3 edge also shows the existence of a small amount of Co^{2+} ions in sample C2 and the region closest to the LSAT substrate.[14,25,26] These changes in the Co-XA spectra are accompanied by a loss of Co-XMCD magnitude. Taken together, we correlate the presence of the non-magnetic/insulating phase with the increased Co^{2+} and Co^{3+} concentrations near the LSCO/LSAT interface.

Under stoichiometric conditions, the Co^{3+}/Co^{4+} ratio is dictated by the Sr doping level. The increase in Co^{2+} and Co^{3+} concentration near the LSCO/LSAT interface indicates that the effective Sr doping and/or oxygen content of the LSCO films differs from the nominal composition. Previous studies using scanning transmission electron microscopy and electron energy loss spectroscopy showed that both the Sr and O concentrations were below the nominal values in a region extending ~10 nm from the $La_{0.5}Sr_{0.5}CoO_3$/STO(001) interface.[17] This composition variation effectively pushes the sample towards the region of the phase diagram where phase separation occurs,[3] such

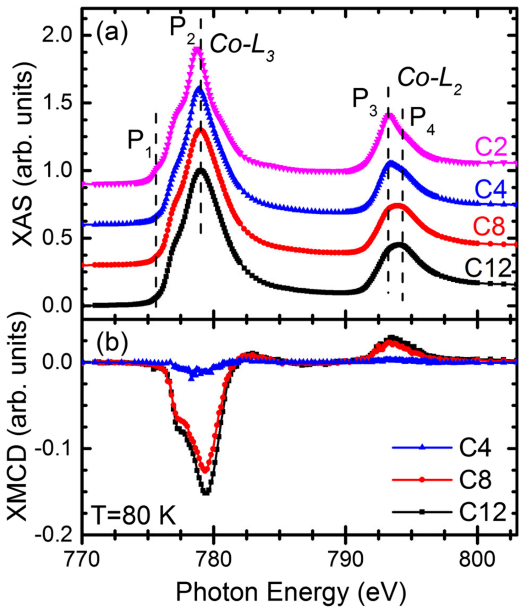

FIG. 5. (a) Co-XA and (b) Co-XMCD spectra for samples C2, C4, C8 and C12 at 80 K. The dashed lines refer to the positions of major features in the Co-XA spectra.

that isolated FM/metallic clusters exist within a non-magnetic/insulating phase. The segregation of Sr ions to the film surface has been explained by thermodynamic considerations related to the energy required to dissolve a Sr ion into $LaCoO_3$,[17,27] while oxygen deficiency has been related to epitaxial strain as the oxygen vacancies form ordered structures to relieve tensile strain.[14,19,28] We postulate that the reduction in epitaxial tensile strain to 0.6% reduces the driving force for oxygen deficiency and thereby the thickness of the phase separated region extends only to ~8 nm from the LSCO/LSAT interface.

In summary, the thickness-dependent magnetic and electrical transport properties of LSCO thin films grown on (001)-oriented LSAT substrates were systematically studied. It was found that in these nearly strain-free thin films, a crossover occurs from FM/metallic to non-magnetic/insulating behavior at a critical thickness of ~8 nm. The change in physical properties is accompanied by differences in the electronic structure of the thin films as evident from XA measurements. This electronic reconstruction is believed to effectively push the system to a lower Sr doping regime characterized by MEPS where isolated FM/metallic clusters form within a non-magnetic/insulating matrix. These results highlight the importance of building a comprehensive understanding of the interactions of the spin, orbital, lattice, and charge degrees of freedom at perovskite oxide interfaces.

ACKNOWLEDGMENTS

This work was supported by the Semiconductor Research Corporation under Task No. 2309.001. The ALS is supported by the Director, Office of Science, Office of Basic Energy Sciences, of the U.S. Department of Energy under Contract No. DE-AC02-05CH11231.

[1] Y. Tokura and N. Nagaosa, Science **288**, 462–468 (2000).
[2] M. A. Senaris-Rodriguez and J. B. Goodenough, J. Solid State Chem. **118**, 323–336 (1995).
[3] J. Wu and C. Leighton, Phys. Rev. B **67**, 174408 (2003).
[4] R. Caciuffo, D. Rinaldi, G. Barucca, J. Mira, J. Rivas, M. A. Senaris-Rodriguez, P. G. Radaelli, D. Fiorani, and J. B. Goodenough, Phys. Rev. B **59**(2), 1068 (1999).
[5] P. L. Kuhns, M. J. R. Hoch, W. G. Moulton, A. P. Reyes, J. Wu, and C. Leighton, Phys. Rev. Lett. **91**, 127202 (2003).
[6] J. Wu, J. W. Lynn, C. J. Glinka, J. Burley, H. Zheng, J. F. Mitchell, and C. Leighton, Phys. Rev. Lett. **94**, 037201 (2005).
[7] D. Phelan, D. Louca, S. Rosenkranz, S.-H. Lee, Y. Qiu, P. J. Chupas, H. Zheng, J. F. Mitchell, J. R. D. Copley, J. L. Sarrao, and Y. Moritomo, Phys. Rev. Lett. **96**, 027201 (2006).
[8] D. Phelan, D. Louca, K. Kamazawa, S.-H. Lee, S. N. Ancona, S. Rosenkranz, Y. Motome, M. F. Hundley, J. F. Mitchell, and Y. Moritomo, Phys. Rev. Lett. **97**, 235501 (2006).
[9] N. X. Phuc, N. Van Khiem, and D. N. H. Nam, J. Magn. Magn. Mater. **242**, 754–756 (2002).
[10] S. Mukherjee, R. Ranganathan, P. S. Anilkumar, and P. A. Joy, Phys. Rev. B **54**(13), 9267–9274 (1996).
[11] M. A. Torija, M. Sharma, M. R. Fitzsimmons, M. Varela, and C. Leighton, J. Appl. Phys. **104**, 023901 (2008).
[12] D. Fuchs, E. Arac, C. Pinta, S. Schuppler, R. Schneider, and H. v. Lohneysen, Phys. Rev. B **77**, 014434 (2008).
[13] D. Fuchs, M. Merz, P. Nagel, R. Schneider, S. Schuppler, and H. von Lohneysen, Phys. Rev. Lett. **111**, 257203 (2013).
[14] W. S. Choi, J.-H. Kwon, H. Jeen, J. E. Hamann-Borrero, A. Radi, S. Macke, R. Sutarto, F. He, G. A. Sawatzky, V. Hinkov, M. Kim, and H. N. Lee, Nano Letters **12**, 4966–4970 (2012).
[15] A. D. Rata, A. Herklotz, K. Nenkov, L. Schultz, and K. Dorr, Phys. Rev. Lett. **100**, 076401 (2008).
[16] M. D. Biegalski, Y. Takamura, A. Mehta, Z. Gai, S. V. Kalinin, H. Ambaye, V. Lauter, D. Fong, S. T. Pantelides, Y. M. Kim, J. He, A. Borisevich, W. Siemons, and H. M. Christen, Advanced Materials Interfaces, 1400203 (2014).
[17] M. A. Torija, M. Sharma, J. Gazquez, M. Varela, C. He, J. Schmitt, J. A. Borchers, M. Laver, S. El-Khatib, and C. Leighton, Adv. Mater. **23**, 2711–2715 (2011).
[18] M. Sharma, J. Gazquez, M. Varela, J. Schmitt, and C. Leighton, Phys. Rev. B **84**, 024417 (2011).
[19] J. Gazquez, S. Bose, M. Sharma, M. A. Torija, S. J. Pennycock, C. Leighton, and M. Varela, APL Materials **1**, 012105 (2013).
[20] J. S. Lee, D. A. Arena, P. Yu, C. S. Nelson, R. Fan, C. J. Kinane, S. Langridge, M. D. Rossell, R. Ramesh, and C. C. Kao, Phys. Rev. Lett. **105**(25), 257204 (2010).
[21] Leptos Manual (Bruker AXS, WI, 2005).
[22] K. Asai, O. Yokokura, N. Nishimori, H. Chou, J. M. Tranquada, G. Shirane, S. Higuchi, Y. Okajima, and K. Kohn, Phys. Rev. B **50**(5), 3025–3032 (1994).
[23] V. G. Prokhorov, Y. P. Lee, K. W. Kim, V. M. Ishchuk, and I. N. Chukanova, Phys. Rev. B **66**(13), 132410 (2002).
[24] H. M. Aarbogh, J. Wu, L. Wang, H. Zheng, J. F. Mitchell, and C. Leighton, Phys. Rev. B **74**(13), 134408 (2006).
[25] M. Merz, P. Nagel, C. Pinta, A. Samartsev, H. von Lohneysen, M. Wissinger, S. Uebe, A. Assmann, D. Fuchs, and S. Schuppler, Phys. Rev. B **82**(17), 174416 (2010).
[26] C. F. Chang, Z. Hu, H. Wu, T. Burnus, N. Hollmann, M. Benomar, T. Lorenz, A. Tanaka, H. J. Lin, H. H. Hsieh, C. T. Chen, and L. H. Tjeng, Phys. Rev. Lett. **102**(11), 116401 (2009).
[27] M. S. D. Read, M. S. Islam, G. W. Watson, F. King, and F. E. J. Hancock, Mater. Chem. **10**, 2298–2305 (2000).
[28] D. O. Klenov, W. Donner, B. Foran, and S. Stemmer, Appl. Phys. Lett. **82**, 3427–3429 (2003).